SLAC–PUB–4794
November 1988
(T/E)

Backgrounds to hadronic Higgs detection in a 1 TeV e^+e^- collider*

ERAN YEHUDAI

Stanford Linear Accelerator Center
Stanford University, Stanford, California 94309

ABSTRACT

We calculate the cross-section of all standard model processes which constitute a potential background to the hadronic decays of an intermediate-mass neutral Higgs in a 1 TeV e^+e^- collider. These calculations are performed taking into account a realistic photon distribution which is due to beamstrahlung. Imposing appropriate kinematic cuts, and looking only at events with a $t\bar{t}$ combination, the Higgs signal is visible, though marginally, above this background.

Submitted to *Physics Letters B*

* Work supported by the Department of Energy, contract DE–AC03–76SF00515.

One of the most important purposes of a TeV scale e^+e^- collider[1,2] is the unveiling of the Higgs sector. A first step towards exploring that sector would be the detection of a neutral Higgs scalar, followed by determination of its production rate and line width. Even if the Higgs signal is clear above its background, precise estimates of that background and identification of cuts that can further increase the signal to background ratio are important for any detailed study of the Higgs particle.

If the Higgs mass is below the W^+W^- threshold, the dominant Higgs decay mode would be into two quarks of the heaviest available flavor. Other decay modes including $H \to \ell^+\ell^-$, $H \to \gamma\gamma$ and $H \to gg$ are much less important. We have to distinguish the case where the Higgs mass is below the $t\bar{t}$ threshold from the case where it is above this threshold. In the second case, the $t\bar{t}$ decay mode dominates the next decay mode ($H \to b\bar{b}$) by a factor of $(m_t/m_b)^2 \approx 100$.

If the Higgs is above the W^+W^- threshold, this channel comes to dominate the decay to $t\bar{t}$. Backgrounds to the W^+W^- channel will be presented elsewhere. Still we extend our calculations to that mass range also, as they might be useful as part of Monte-Carlo simulations of the e^+e^- collider environment.

Higgs decay into two quarks has the experimental signature of two hadronic jets with invariant mass close to that of the Higgs, plus missing energy. This paper presents a systematic calculation of the cross-section of the main processes having experimental signature similar to that of hadronic Higgs decay.

Radiated photons play a very significant role in a TeV scale e^+e^- accelerator. Although classical breamsstrahlung remains important, a much larger effect[3] arises from the synchrotron radiation emitted by electrons in one beam due to the electric field it experiences as it passes through the other beam; this radiation is termed "beamstrahlung". A quantitative comparison of these two effects is given below. To the best of our knowledge, this is the first time such backgrounds have been computed with a realistic photon spectrum. Previous calculations were usually done taking only bremsstrahlung photons into consideration, and therefore

give substantially smaller results for photon-induced processes.

In order to account for the photon radiation in a systematic way, we treat each beam as being composed of both electrons (or positrons) and (real and virtual) photons. We therefore look at processes with both electrons and photons as initial particles. We distinguish between photon-initiated processes and electron-initiated processes containing a virtual photon by insisting that in the later process the photon carries a nontrivial momentum perpendicular to the beam direction. The process illustrated in figure 1, for example, is classified as $e^-\gamma \to e^-q\bar{q}$ if the perpendicular momentum of the indicated photon is larger than some cutoff to be chosen later. Otherwise the same process is considered $\gamma\gamma \to q\bar{q}$.

The processes we calculate are:

1. $e^+e^- \to q\bar{q}$
2. $\gamma\gamma \to q\bar{q}$
3. $e^+e^- \to q\bar{q}\gamma$
4. $e^+e^- \to q\bar{q}Z_0 \to q\bar{q}\nu\bar{\nu}$
5. $\gamma e^- \to q\bar{q}e^- + (\text{c.c.})$
6. $\gamma e^- \to q\bar{q}\nu + (\text{c.c.})$

In the following discussion, s is the collider center of mass energy squared, $\hat{s}$ is the center of mass energy squared of the two incoming particles, s' is the invariant mass squared for the $q\bar{q}$ system, $p_\perp$ is the perpendicular momentum of that system, and $p_\perp^1$ and $p_\perp^2$ are the perpendicular momenta of the quark and anti-quark respectively. Cross-sections are presented in units of the point cross-section R, where

$$1R = \frac{4\pi\alpha^2}{3s} = \frac{86.8 \text{ fb}}{(E_{\text{CM}}(\text{TeV}))^2}. \tag{1}$$

In this paper we consider only the WW fusion channel for Higgs production

(figure 2). This channel is dominant for high energy e^+e^- colliders.[4,5] The calculation of the Higgs production rate through this process is illustrated below.

The Higgs is treated in the narrow-resonance approximation, that is, we take the invariant mass dependence of the Higgs products to have the form

$$\frac{d\sigma}{dm^2} \approx \frac{1}{\Gamma^2 + (m - m_H)^2} \tag{2}$$

where Γ is the greater of the Higgs decay width and the experimental resolution, here taken to be 20 GeV. This procedure gives approximately the same results as calculating the process $e^+e^- \to q\bar{q}\nu\bar{\nu}$, with the two outgoing quarks of opposite chirality.[6] The approximation is valid as long as the Higgs width is not too large, and as long as the calculation is done not too far from the Higgs peak ($\Gamma^2, (m - m_H)^2 \ll m_H^2$).

The cross-sections to be presented are calculated using spinor techniques.[7] These involve calculating the matrix element for each Feynmann diagram and polarization combination separately, rather than averaging over polarizations. These techniques are particularly convenient when many diagrams are associated with each process (up to 8 in some cases here), and when the fermions involved can be taken to be massless (here all fermions with the exception of the top quark are indeed taken to be massless).

As an illustration of the methods used here, we present the main steps in the calculation of the cross-section of the Higgs production process $e^+e^- \to H\nu\bar{\nu}$. This process is particularly simple because only left-handed, light fermions are involved. Further, since only one Feynmann diagram contributes to the process, the explicit spinor products do not appear in the final expression. The differential cross-sections for the other processes are too complicated to present here, but are available upon request from the author.

For momenta labelled as in Fig. 2, the matrix element for $e^+e^- \to H\nu\bar{\nu}$ is

$$\begin{aligned}\mathcal{M} &= \left\{\bar{u}_L(p_3)\frac{-ig}{\sqrt{2}}\gamma^\mu u_L(p_1)\right\}\frac{-ig_{\mu\nu}}{t_{13}-m_W^2}(ig^{\nu\tau}m_W g) \\ &\quad\times\frac{-ig_{\tau\sigma}}{t_{24}-m_W^2}\left\{\bar{u}_L(p_2)\frac{-ig}{\sqrt{2}}\gamma^\sigma u_L(p_4)\right\} \\ &= \frac{ig^3 m_W t(3,2)s(4,1)}{(t_{13}-m_W^2)(t_{24}-m_W^2)}\end{aligned} \tag{3}$$

where

$$\begin{aligned}t_{nm} &= (p_n-p_m)^2, \\ t(n,m) &= t(p_n,p_m) = \bar{u}_L(p_n)u_R(p_m), \\ s(n,m) &= s(p_n,p_m) = \bar{u}_R(p_n)u_L(p_m).\end{aligned} \tag{4}$$

The spinor products $t(p,p')$, $s(p,p')$ satisfy $|t(p,p')|^2 = |s(p,p')|^2 = 2p\cdot p'$. Thus the final expression for the Higgs production cross-section (in units of R) can be written simply as

$$\begin{aligned}\sigma &= \int \frac{1}{4}\frac{3s}{4\pi\alpha^2}\frac{(2\pi)^4}{2s}\sum_{\text{pol.}}|\mathcal{M}|^2 d\Phi_3(p_1+p_2;\,p_3,p_4,p_5) \\ &= \int \frac{3\alpha m_W^2/s}{2^9\pi^2\sin^6\theta_W}\frac{t_{32}t_{14}}{(t_{13}-m_W^2)^2(t_{24}-m_W^2)^2} \\ &\quad\times\sqrt{s^2+m_H^4+m_{34}^4-2sm_H^2-2sm_{34}^2-2m_H^2m_{34}^2}\;\,d\Omega\,d\cos\theta\,dm_{34}^2.\end{aligned} \tag{5}$$

where θ is the angle between the Higgs particle and the beam direction, and Ω describes the direction of the ν in the $\nu\bar{\nu}$ c.m. frame.

In eq. (5) and in our other calculations, phase space integration over multi-particle final states is performed making repeated use of the relation

$$d\Phi_n(P;\, p_1, p_2, \ldots, p_n) = d\Phi_{n-1}(P;\, p_{12}, p_3, \ldots, p_n) d\Phi_2(p_{12};\, p_1, p_2)(2\pi)^3 dm_{12}^2. \quad (6)$$

In particular this method allows a simple extraction of the differential cross-section $d\sigma/ds'$ in processes of the form $X \to q\bar{q}\, Y$ with s' the invariant mass squared of the $q\bar{q}$ system. The integration is performed numerically using a Monte-Carlo multi-dimensional adaptive integration procedure, VEGAS[8]. Figure 3 shows the total cross-section for $e^+e^- \to \nu\bar{\nu}H$ as a function of m_H, computed from eq. (5) and ignoring all initial photon radiation.

In calculating the initial photon and electron spectrum, one has to distinguish between bremsstrahlung and beamstrahlung. Bremsstrahlung depends only on the beam energy, and is parametrized to first order by the Weizsacker-Williams distribution functions

$$\begin{aligned} f_\gamma(x) &= \frac{\alpha \log(s/m_e^2)}{2\pi} \frac{1+(1-x)^2}{x} \\ f_e(x) &= \frac{\alpha \log(s/m_e^2)}{2\pi} \frac{1+x^2}{1-x} + I\delta(1-x) \end{aligned} \quad (7)$$

where I is such that $\int_0^1 f_e(x)\, dx = 1$.

The effect of beamstrahlung is not decomposable to distribution functions. We thus parametrize beamstrahlung in terms of luminosity functions expressing the effective collision luminosity as a function of the fraction of total s involved in the collision. Beamstrahlung depends heavily on machine parameters such as luminosity, pulse rate and bunch geometry.[9-12] Here we use the following set of accelerator parameters, with the terminology as in reference 12:

$$C = 0.3, \quad G = 5.00 \text{ and } Y = 1600. \quad (8)$$

These correspond to a bunch length $\ell_0 \sim 0.4mm$, and a luminosity per pulse $\mathcal{L} \sim 10^{31} cm^{-2}$ (to determine the physics luminosity, multiply $\mathcal{L}$ by the repetition

rate, of order 100/sec.). The cross-section of the bunches is assumed to be elliptical with a_x and a_y as the semi-major and semi-minor axes, and $a_x/a_y = 100$.

The cross-section for each process is then folded together with the appropriate luminosity function using

$$\sigma_{\rm tot} = \frac{1}{s}\int \sigma(\hat{s}) \cdot \mathcal{L}(\hat{s}) d\hat{s}, \tag{9}$$

where $\hat{s}$ is the center of mass energy squared of the initial two particle system, and $\mathcal{L}(\hat{s})$ is the relative luminosity for a collision having center of mass energy squared $\hat{s}$. Figure 4 shows the luminosity functions used here which include beamstrahlung effects, as well as the corresponding luminosity functions without beamstrahlung. The functions are normalized so that the total area under the curve $\mathcal{L}_{ee}$ is 1.

The Feynmann diagrams contributing to processes 1-6 are illustrated in figure 5. The propagators marked with arrows are those that can go on shell, creating collinear divergences.

As any of the propagators marked by 'a' go on shell, the direction of at least one of the quarks becomes close to that of the beam. These divergences can be avoided by imposing cuts on the quark transverse momenta $p_\perp^1, p_\perp^2 > p_\perp'^{\rm min}$, with $p_\perp'^{\rm min}$ on the order of a few GeV (here we use $p_\perp'^{\rm min} = 5$ GeV, which corresponds to an angle of roughly $1° - 3°$ between the quark and the beam direction). In practice the quark jets removed by the cut are close to the beam pipe, thus escaping detection. Events of this type appear as one jet plus missing energy; we do not consider that signature here.

As the propagators marked by 'b' go on shell, the total $p_\perp$ of the $q\bar{q}$ system tends to 0. This gives a large leading-log contribution to the cross-section (see figure 6), which however can be completely eliminated by imposing a cut on the perpendicular momentum of the $q\bar{q}$ system — $p_\perp > p_\perp^{\rm min}$. Figure 7 shows the differential cross-section $\frac{d\sigma}{dp_\perp}$ of a typical background process ($\gamma e \rightarrow q\bar{q}e$) compared with that of the Higgs production. We choose a cut at $p_\perp^{\rm min} = 50$ GeV.

Having imposed those cuts, all remaining processes have a 3-particle final state:

1. $e^+e^- \to q\bar{q}\gamma$
2. $\gamma e \to q\bar{q}e$
3. $\gamma e \to q\bar{q}\nu$
4. $e^+e^- \to q\bar{q}Z_0$

The first two processes are related by crossing symmetry. Their most distinctive feature is the presence of an additional, isolated, high $p_\perp$ visible particle: photon in the case of process 1 and electron in process 2. Rejection of events with an isolated high $p_\perp$ track in the opposite hemisphere to the jets reduces these processes as a background to Higgs detection. However, cases in which the extra particle, though visible in principle, escapes detection by falling too close to the beam pipe occur with a large cross-section, and must be considered here. The cross-section for these processes is given in figure 8, where we follow reference 1 in estimating that no detection is possible within 10° of the beam. As can be seen in the figure, these signals are large enough to obscure the Higgs peak for $100\,\mathrm{GeV} < m_H < 250\,\mathrm{GeV}$.

The last class of events are those having the phenomenological signature of two hadronic jets, with large $p_\perp$, and no visible track in the opposite hemisphere. These include $\gamma e \to q\bar{q}\nu$ and $\gamma e \to q\bar{q}Z_0$ (with the Z_0 subsequently decaying to two ν's), but also $\gamma e \to q\bar{q}e$ and $\gamma e \to q\bar{q}\gamma$ with the third particle escaping detection. Figure 9 compares the combined cross-section for these processes and those in which the visible particle escapes detection with that of the Higgs signal under similar cuts. The Higgs signal is still lower than these backgrounds.

A further enhancement of the Higgs signal relative to its background can be achieved if jets following the production of a top quark are distinguishable from jets due to light quarks. Figure 10 shows the cross section for a final state involving a $t\bar{t}$ combination (assuming $m_t = 60\,\mathrm{GeV}$). It is reasonable[13] to assume that a top jet can be distinguished from a light jet, either based on the invariant mass of the jet or by looking for a large number of sub-jets. If the Higgs mass is above

the two top threshold, virtually all Higgs particles decay into two top quarks, and thus looking at those events in which both jets are identified as top jets leaves a clearly visible Higgs signal.

Finally, one can use the measurable angular distribution of the visible electrons in the process $e\gamma \to t\bar{t}e$ to estimate the size of the signal for the same process with the electron escaping detection. Figure 11 shows the angular distribution of electrons from the process $e\gamma \to t\bar{t}e$ compared with the Higgs signal. Note that though the signal for angles larger than 10° comprises only about 10% of the total cross-section, comparing our predictions with experimental results in that range can confirm our estimate for that part of the background which is experimentally indistinguishable from the Higgs signal.

If on the other hand the Higgs mass is below the two top threshold, the Higgs decays mainly into two bottom quarks. A bottom jet is hardly distinguishable from a jet of a lighter quark based on kinematics alone, but a vertex detector might allow at least a statistical discrimination. In that case though, the background would be lower, due to the smaller electromagnetic cross-section of the bottom quark.

In conclusion we see that under a reasonable set of cuts: $p_\perp^1, p_\perp^2 > p_\perp'^{\min}$, $p_\perp > p_\perp^{\min}$, no visible track in opposite hemisphere, and looking only for t (or b if the t is too heavy) jet events, the Higgs signal can be separated from all conventional backgrounds, with signal to noise ratio of about 2:1.

Acknowledgements:

I am grateful to M. Peskin for suggesting this topic, for instructive discussions, and for critically reading the manuscript. I also thank R. Blankenbecler for useful discussions, and in particular for supplying the photon spectrum used here.

FIGURE CAPTIONS

1) Process considered as either $e^-\gamma \to e^- q\bar{q}$ or $\gamma\gamma \to q\bar{q}$.

2) Feynmann diagram for $e^+e^- \to \nu\bar{\nu}H$.

3) Total cross-section for $e^+e^- \to \nu\bar{\nu}H$ as a function of m_H.

4) Luminosity functions with and without the effects of beamstrahlung (bins at $x = 0$ and $x = 1$ are not shown despite carrying nontrivial weight.)

5) Feynmann diagrams for: (a) $e^+e^- \to q\bar{q}$. (b) $\gamma\gamma \to q\bar{q}$. (c) $e\gamma \to q\bar{q}e$. (d) $e\gamma \to q\bar{q}\nu$. (e) $e^+e^- \to q\bar{q}\gamma$. (f) $ee \to q\bar{q}Z_0 \to q\bar{q}\nu\bar{\nu}$.

6) Differential cross-section for $\gamma\gamma \to q\bar{q}$ *vs.* $e^+e^- \to H\nu\bar{\nu}$ as a function of the invariant mass of the $q\bar{q}$ or Higgs system. Here and henceforth, we show Higgs production cross-sections for Higgs mass of 100, 150 and 200 GeV. ($e^+e^- \to q\bar{q}$ cross-section is too small to show.)

7) Differential cross-section for $\gamma e \to q\bar{q}e$ *vs.* $e^+e^- \to H\nu\bar{\nu}$ as a function of perpendicular momentum of the $q\bar{q}$ or Higgs system. Higgs mass is taken to be 150 GeV.

8) Differential cross-section for processes with visible extra particles at more than 10° from the beam. Here and henceforth, a cutoff at $p_\perp = 50$ GeV is imposed.

9) Differential cross-section for processes with no visible extra particle present at more than 10° from the beam.

10) Differential cross-section for $e^+e^- \to t\bar{t}$ + (undetected particles) *vs.* $e^+e^- \to H\nu\bar{\nu}$.

11) Angular distribution of electrons from $e\gamma \to t\bar{t}e$ with $t\bar{t}$ invariant mass of 150 GeV, compared with the $e^+e^- \to H\nu\bar{\nu}$ signal with $m_H = 150$ GeV. The Higgs signal is spread over 5° and 10°.

REFERENCES

1. C. Ahn *et.al.*, SLAC-Report-329 (1988).
2. G. Altarelli, in *Proceedings of the Workshop on Physics at Future Accelerators*, La Thuile(Italy) and Geneva(Switzerland) CERN 87-07 (1987).
3. G.J. Feldman, in *Proceedings of the Fifteenth SLAC Summer Institute on Particle Physics*, E.C. Brennan, ed. SLAC Report No. 328 (1987).
4. D.R.T. Jones, S.T. Petcov, *Phys. Lett.* **84B**(1979), 440.
5. R.N. Cahn, S. Dawson, *Phys. Lett.* **136B**(1984), 196.
6. Note that the diagram involving the Higgs boson is the only one contributing to $e^+e^- \to q\bar{q}\nu\bar{\nu}$ with the two quarks having opposite chirality, as all vector-fermion vertices conserve chirality.
7. R. Kleiss, W.J. Stirling, *Nucl. Phys.* **B262**(1985), 235.
8. G.P. Lepage, *Jr. Comp. Phys.* **27**(1978), 192, G.P. Lepage, CLNS-80/447 (1980).
9. P.B. Wilson, SLAC-PUB-3985 (1986).
10. R. Blankenbecler and S.D. Drell, *Phys. Rev.* **D36**(1987), 277.
11. P. Chen, in *Proceedings of the Workshop on Physics at Future Accelerators*, La Thuile(Italy) and Geneva(Switzerland) CERN 87-07 (1987).
12. R. Blankenbecler and S.D. Drell, *Phys. Rev.* **D37**(1988), 3308.
13. P.R. Burchat, D.L. Burke and A. Petersen, SLAC-PUB-4638(1988).

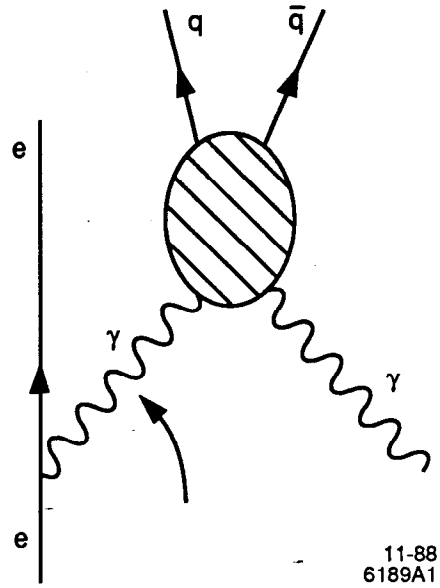

Fig. 1

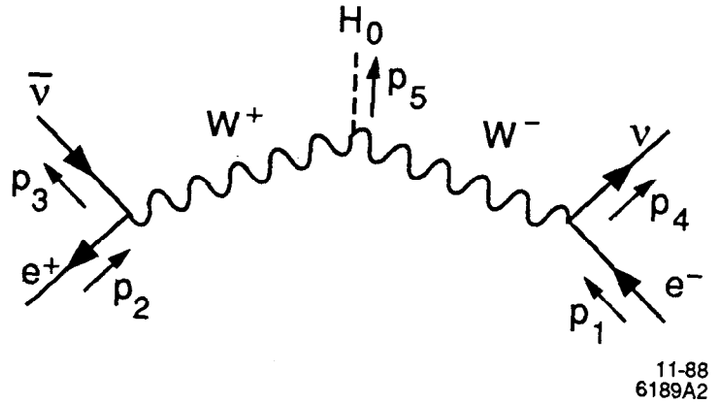

Fig. 2

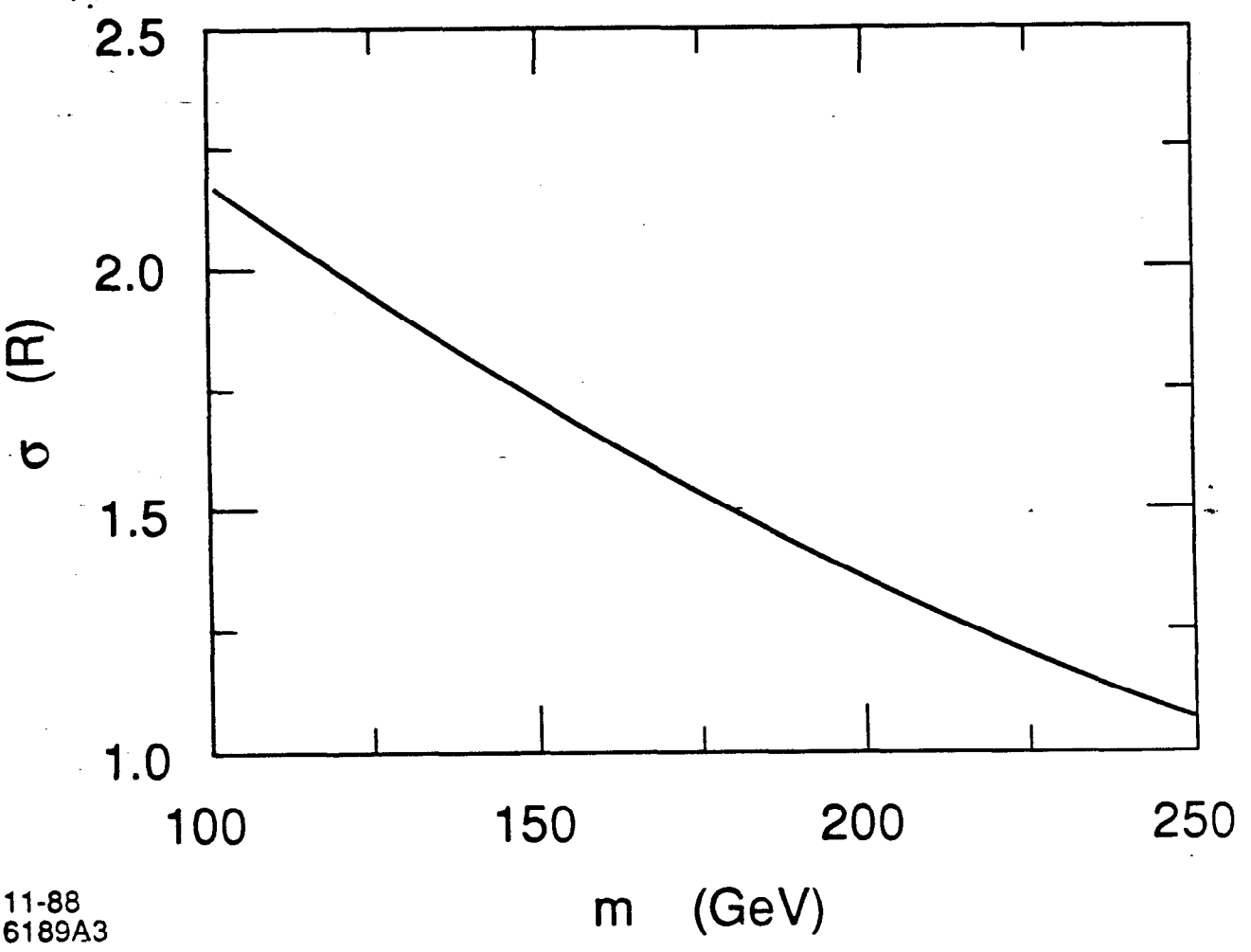

Fig 3

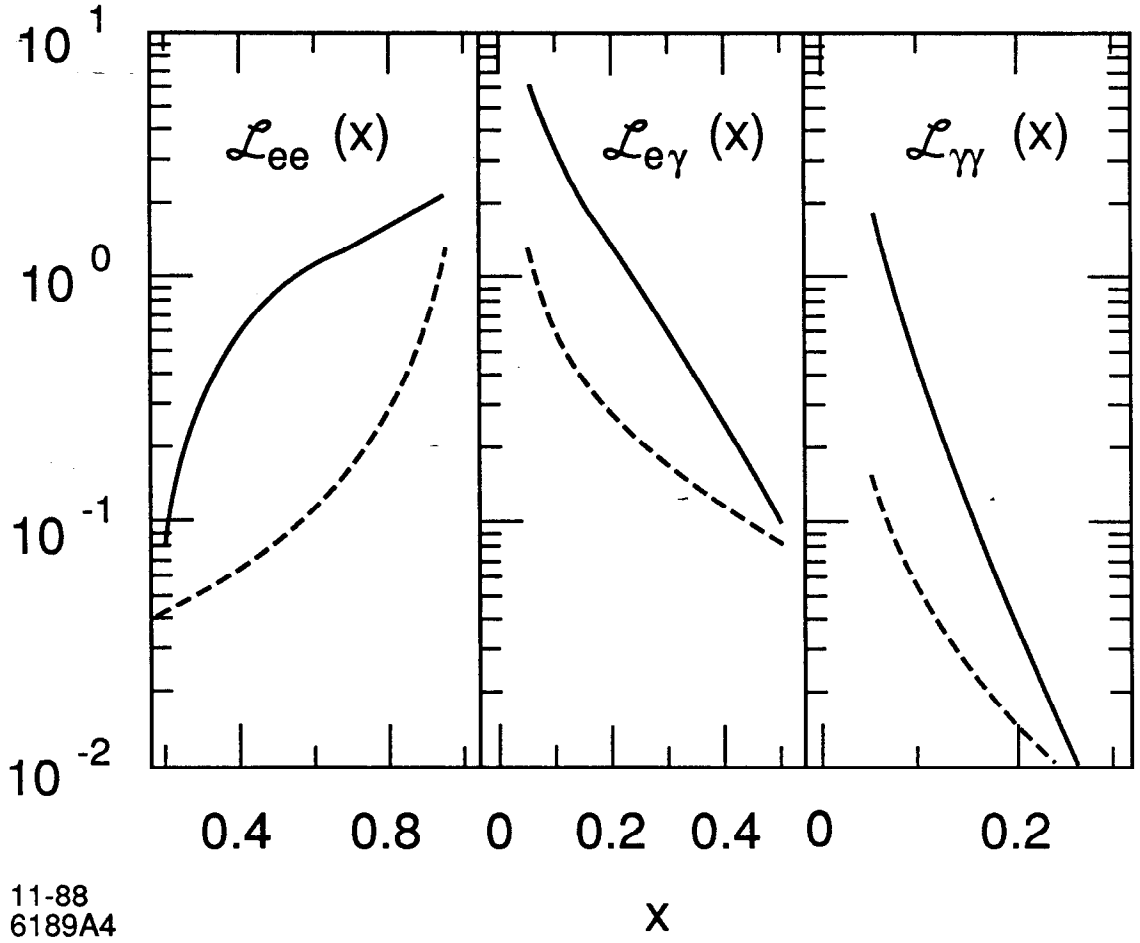
10^{1}
10^{0}
10^{-1}
10^{-2}
$\mathcal{L}_{ee}$ (x)
$\mathcal{L}_{e\gamma}$ (x)
$\mathcal{L}_{\gamma\gamma}$ (x)
0.4
0.8
0
0.2
0.4
0
0.2
x
11-88
6189A4

Fig. 4

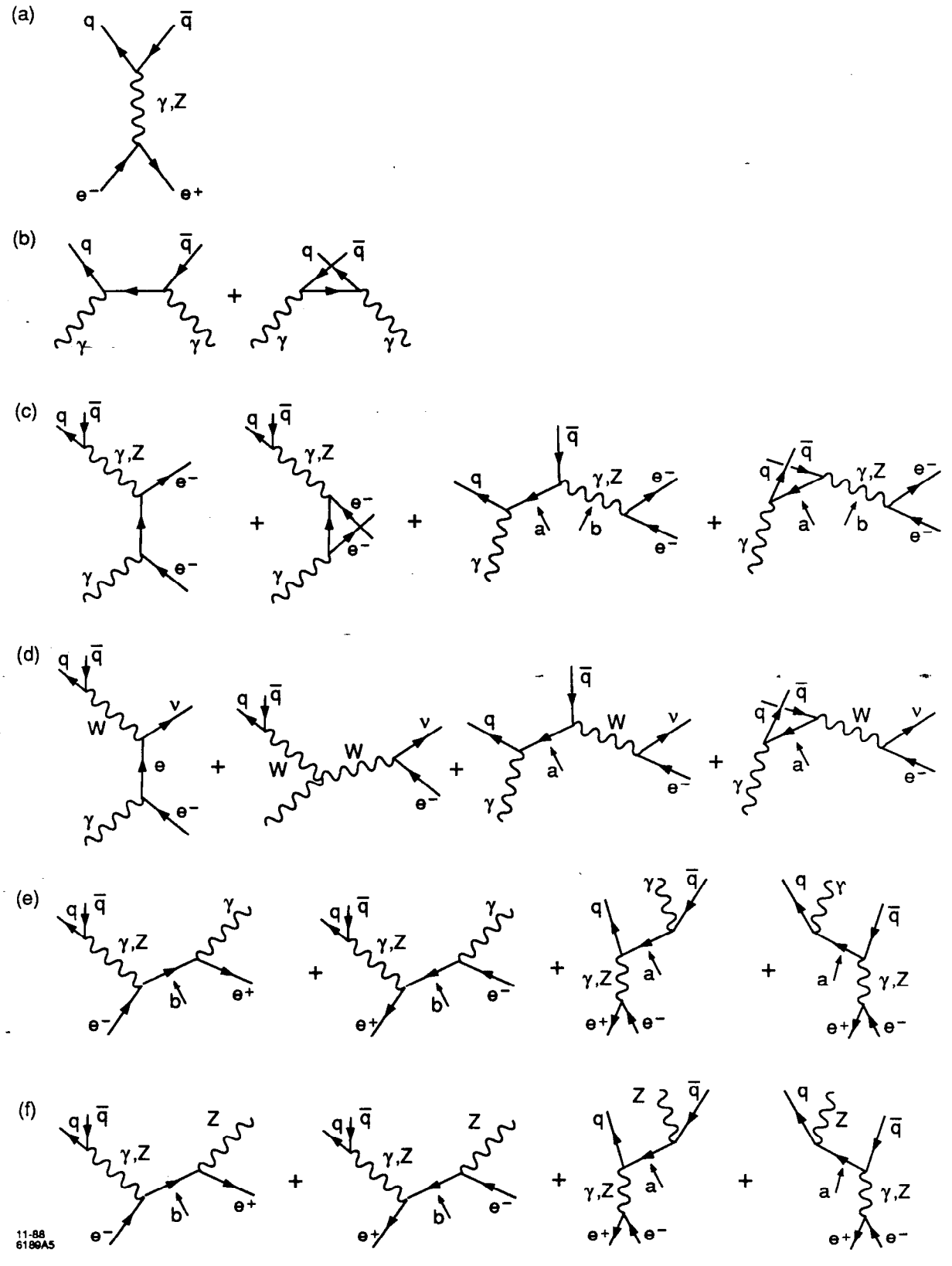
(a)
q
q̄
γ,Z
e⁻
e⁺
(b)
q
q̄
γ
γ
+
q
q̄
γ
γ
(c)
q
q̄
γ,Z
e⁻
e⁻
γ
+
q
q̄
γ,Z
e⁻
e⁻
γ
+
q̄
q
γ,Z
e⁻
a
b
e⁻
γ
+
q
q̄
γ,Z
e⁻
a
b
e⁻
γ
(d)
q
q̄
W
ν
e
e⁻
γ
+
q
q̄
W
W
ν
e⁻
+
q̄
q
W
ν
a
e⁻
γ
+
q
q̄
W
ν
a
e⁻
γ
(e)
q
q̄
γ,Z
γ
b
e⁻
e⁺
+
q
q̄
γ,Z
γ
b
e⁺
e⁻
+
γ
q̄
q
γ,Z
a
e⁺
e⁻
+
q
γ
q̄
a
γ,Z
e⁺
e⁻
(f)
q
q̄
γ,Z
Z
b
e⁻
e⁺
+
q
q̄
γ,Z
Z
b
e⁺
e⁻
+
Z
q̄
q
γ,Z
a
e⁺
e⁻
+
q
Z
q̄
a
γ,Z
e⁺
e⁻
11-88
6189A5

Fig 5

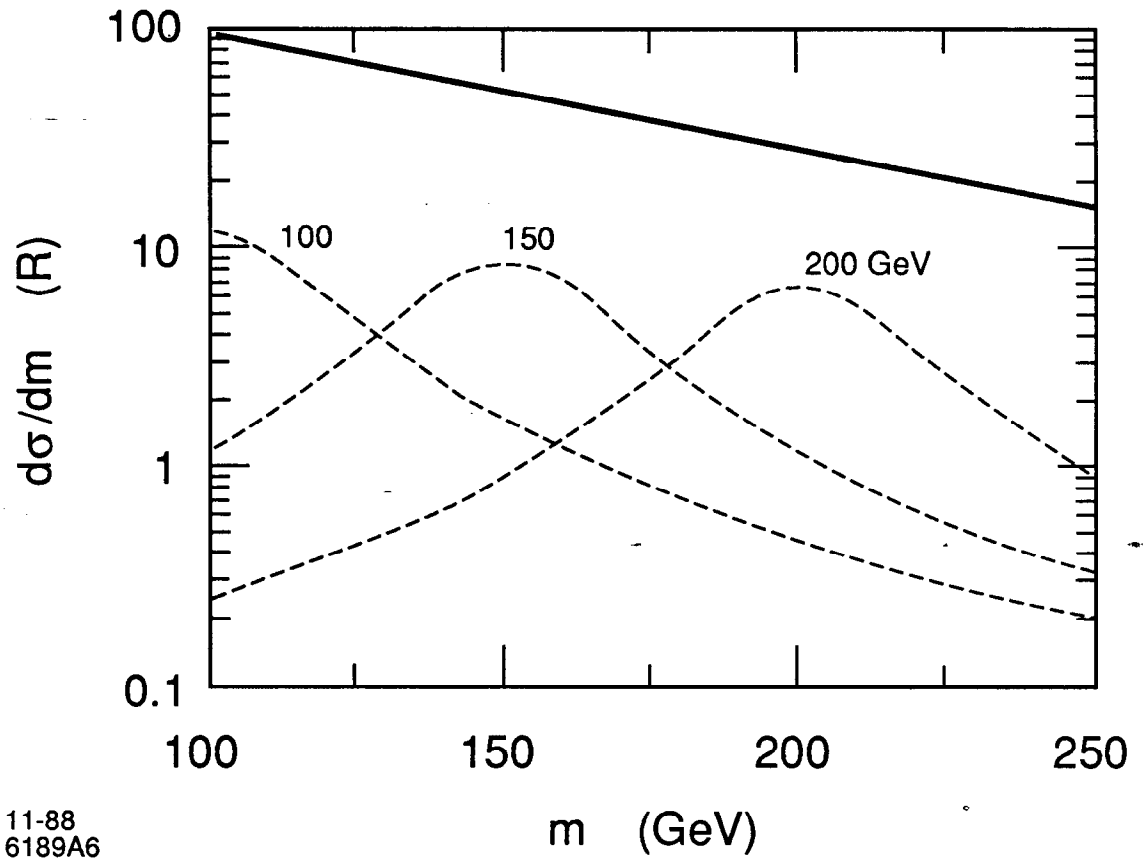
100
10
1
0.1
dσ/dm (R)
100
150
200 GeV
100
150
200
250
m (GeV)
11-88
6189A6

Fig. 6

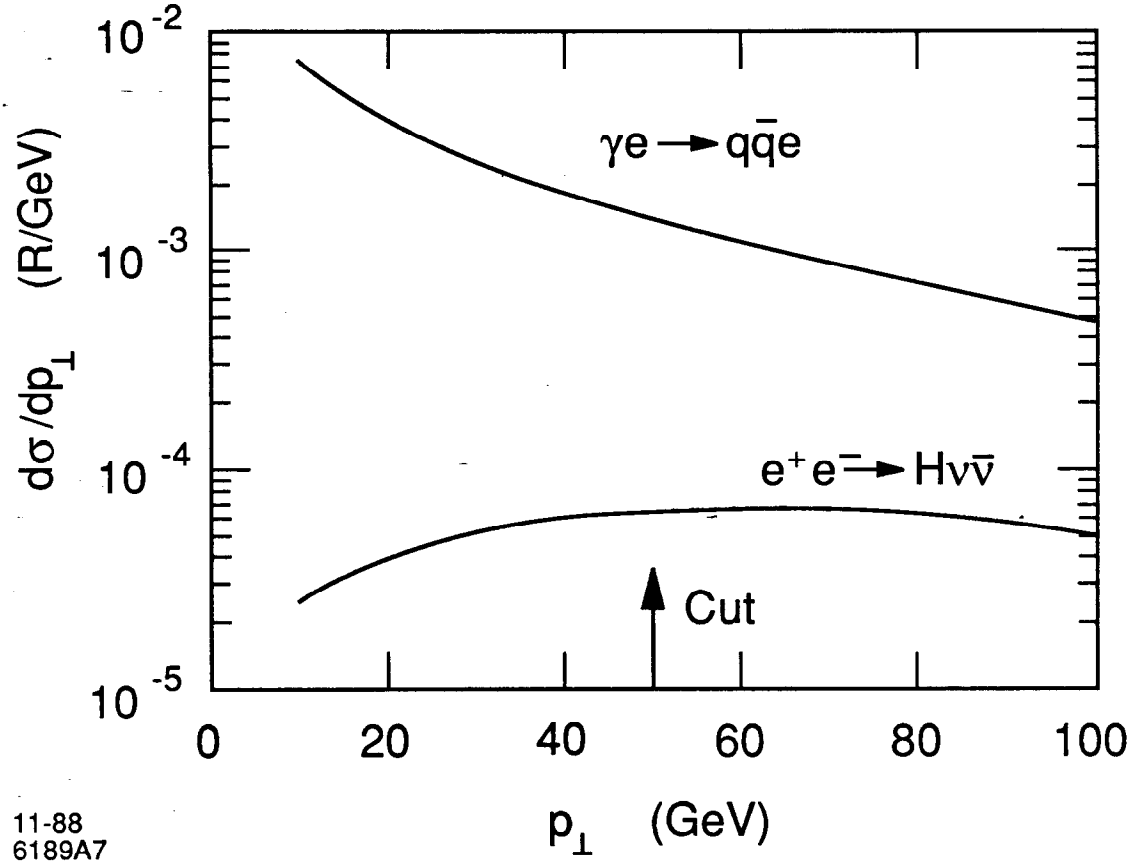
10^{-2}
10^{-3}
10^{-4}
10^{-5}
$d\sigma/dp_\perp$ (R/GeV)
$\gamma e \rightarrow q\bar{q}e$
$e^+e^- \rightarrow H\nu\bar{\nu}$
Cut
0
20
40
60
80
100
$p_\perp$ (GeV)
11-88
6189A7

Fig. 7

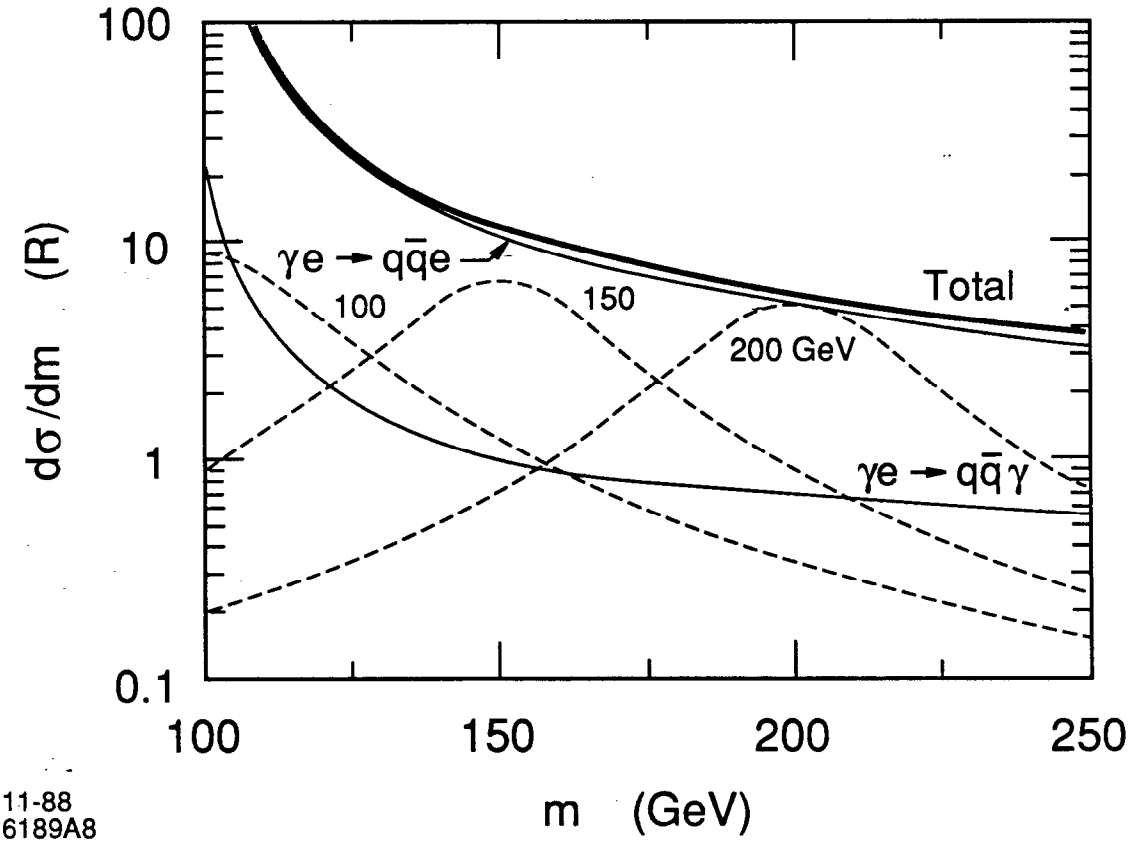
100
10
1
0.1
dσ/dm (R)
γe → qq̄e
100
150
200 GeV
Total
γe → qq̄γ
100
150
200
250
m (GeV)
11-88
6189A8

Fig 8

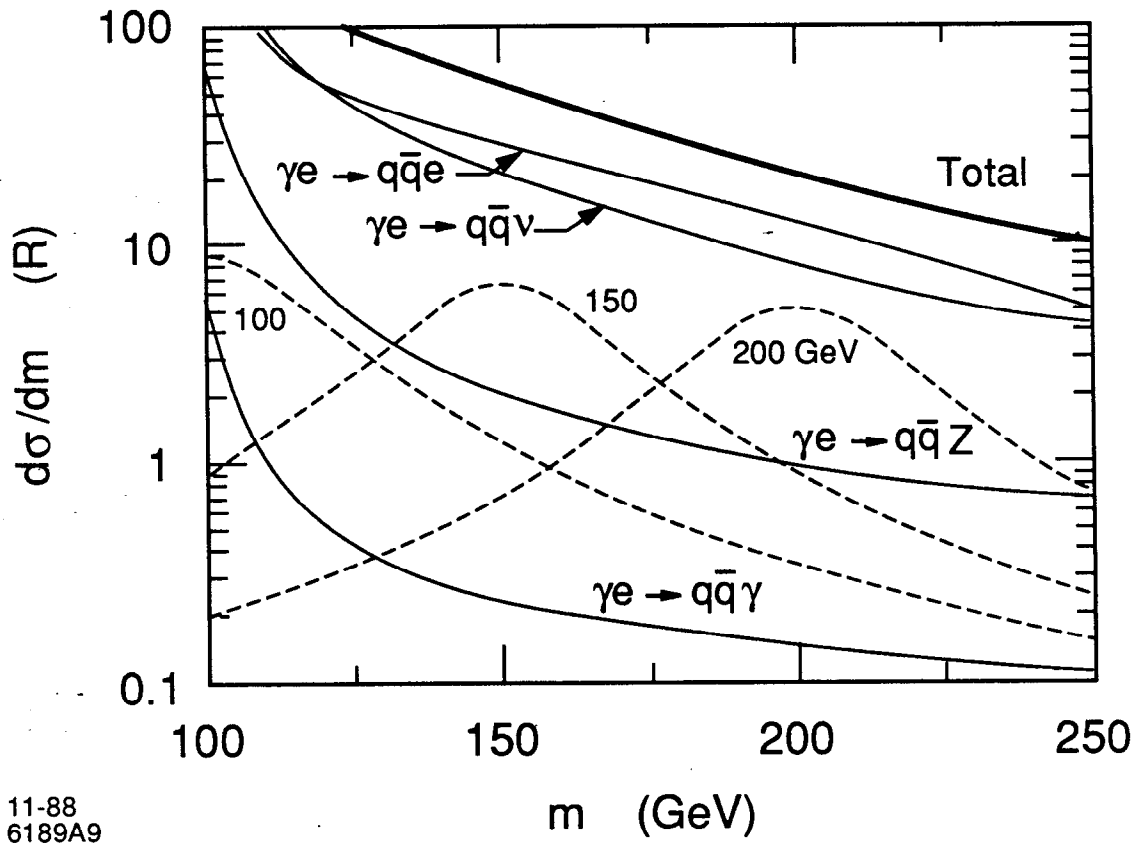
100
10
1
0.1
dσ/dm (R)
γe → qq̄e
γe → qq̄ν
Total
100
150
200 GeV
γe → qq̄Z
γe → qq̄γ
100
150
200
250
m (GeV)
11-88
6189A9

Fig. 9

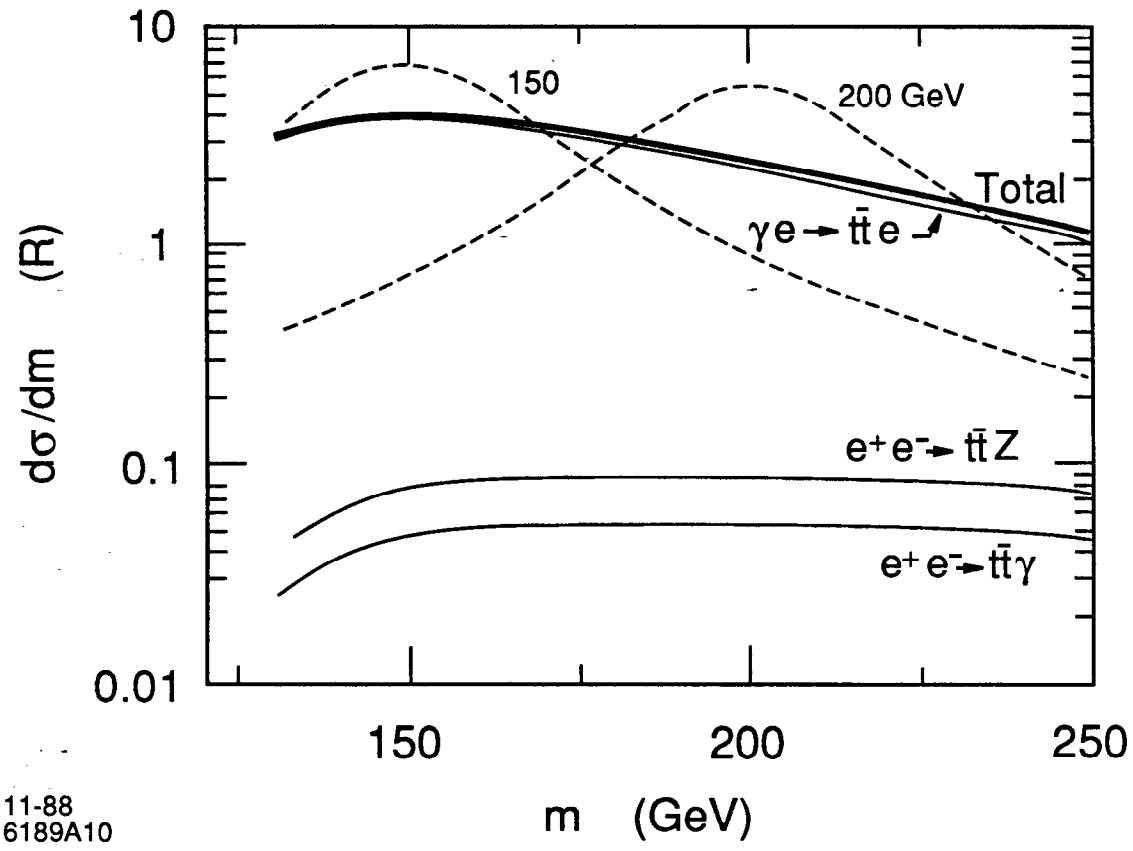

11-88
6189A10

Fig. 10

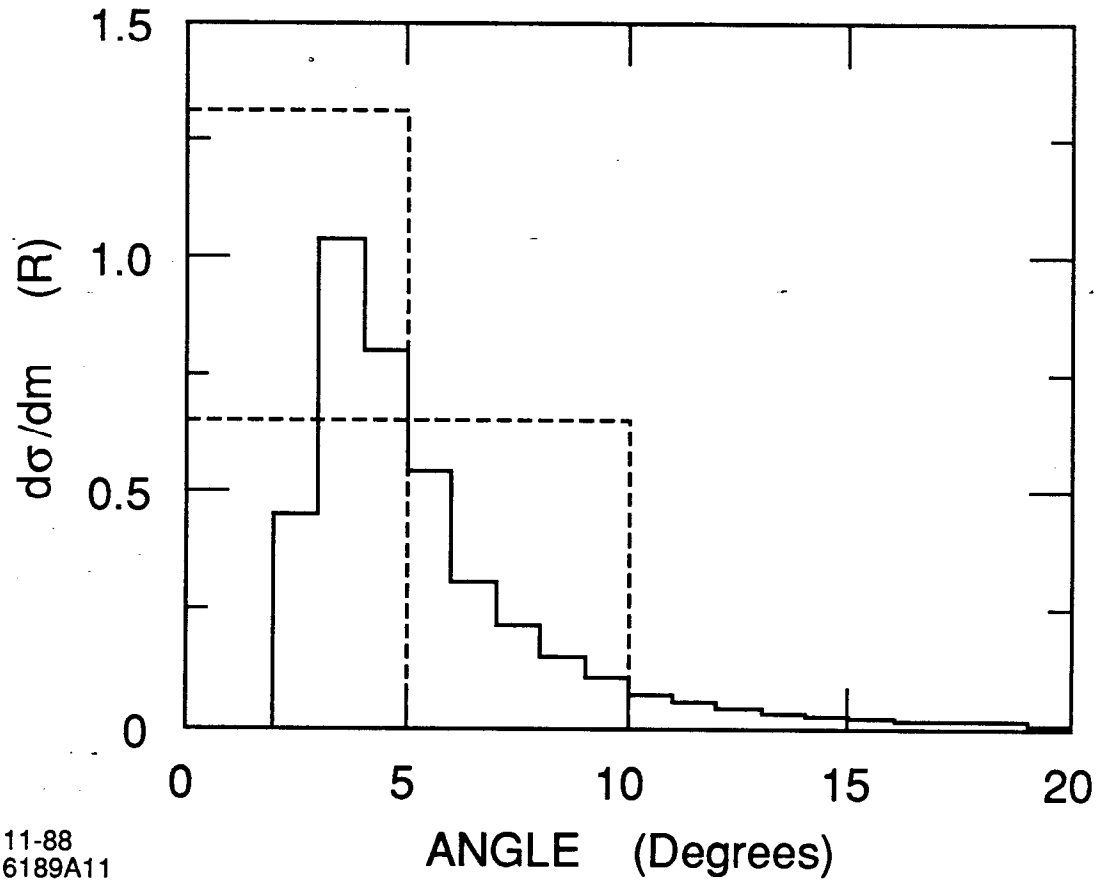

Fig. 11